

Apparent delay of the Kibble-Zurek mechanism in quenched open systems

Roy D. Jara Jr.* and Jayson G. Cosme†

National Institute of Physics, University of the Philippines, Diliman, Quezon City 1101, Philippines

(Dated: August 22, 2024)

We report an intermediate regime in the quench time, τ_q , separating the usual validity of the Kibble-Zurek mechanism (KZM) and its breakdown for rapid quenches in open systems under finite quench protocols. It manifests in the power-law scaling of the transition time with τ_q as the system appears to enter the adiabatic regime, even though the ramp is already terminated and the final quench value is held constant. This intermediate regime, which we dub the delayed KZM, emerges due to the dissipation, preventing the system from freezing in the impulse regime. This results in a large delay between the actual time the system undergoes a phase transition and the time inferred from a threshold-based criterion for the order parameter, as done in most experiments. We demonstrate using the open Dicke model and its one-dimensional lattice version that this phenomenon is a generic feature of open systems that can be mapped onto an effective coupled oscillator model. We also show that the phenomenon becomes more prominent near criticality, and its effects on the transition time measurement can be further exacerbated by large threshold values for an order parameter. Due to this, we propose an alternative method for threshold-based criterion which uses the spatiotemporal information, such as the system's defect number, for identifying the transition time.

I. INTRODUCTION

Initially formulated to describe the evolution of topological defects in the early universe [1–3], the Kibble-Zurek Mechanism (KZM) has been successful in describing the dependence of the defect number and duration of a continuous phase transition on the quench timescale, τ_q [4]. In particular, the theory has been tested in multiple platforms, ranging from atomic Bose-Einstein condensates [5–13], spin systems [14–17], Rydberg atom setups [18, 19], and trapped-ion systems [20, 21]. It has also been tested in dissipative quantum systems [17, 22–28], and has recently been extended to include generic nonequilibrium systems [29–31].

Under the standard KZM, a generic closed system with a continuous phase transition has a diverging relaxation time, τ , and correlation length, ξ , as it approaches its critical point, λ_c . In particular, one expects τ and ξ to scale as $\tau \propto |\varepsilon|^{-vz}$ and $\xi \propto |\varepsilon|^{-v}$ [4], respectively, where $\varepsilon = (\lambda - \lambda_c)/\lambda_c$ is the reduced distance of the control parameter, λ , from the critical point, while v and z are the static and dynamic critical exponents, respectively. It is then expected that if the system is linearly quenched via a ramp protocol, $\varepsilon = t/\tau_q$, the system will become frozen near λ_c due to τ diverging. This motivates the introduction of the adiabatic-impulse (AI) approximation, where the system's dynamics are classified into two regimes [4]. Far from λ_c , the system is in an adiabatic regime, in which its macroscopic quantities adiabatically follow the quench. Near λ_c , the system enters the impulse regime, wherein all relevant observables remain frozen even after passing λ_c . It only reenters the adiabatic regime and transitions to a new phase after some finite time referred

to as the freeze-out time, \hat{t} , has passed [4]. This occurs after the system reaches the AI crossover point, $\varepsilon(\hat{t})$, setting $\hat{t} \sim \tau(\varepsilon(\hat{t}))$ [4]. The KZM predicts that, due to the scaling of τ , \hat{t} and $\varepsilon(\hat{t})$ must follow the scaling laws [4]

$$\hat{t} \propto \tau_q^{\frac{vz}{1+vz}}, \quad \varepsilon(\hat{t}) \propto \tau_q^{-\frac{1}{1+vz}}. \quad (1)$$

While the standard KZM has been successful in explaining the dynamics of continuously quenched systems, studies on systems with finite quenches have shown that the mechanism breaks down if the quench terminates quickly at a certain value, ε_f [32–40]. In particular, \hat{t} and $\varepsilon(\hat{t})$ saturate at a finite value as $\tau_q \rightarrow 0$, with $\varepsilon(\hat{t}) = \varepsilon_f$, and thus $\hat{t} \sim \tau(\varepsilon_f)$ [40]. In Ref. [40], this breakdown of the KZM is predicted to occur at some critical quench time $\tau_{q,c} = \hat{t}_{\text{fast}}/\varepsilon_f$, where \hat{t}_{fast} is the saturation value of \hat{t} in the sudden quench limit, $\tau_q \rightarrow 0$.

Measuring the exact value of \hat{t} and $\varepsilon(\hat{t})$ is a nontrivial task unlike defect counting due to the limitations in detecting the exact time a system reenters the adiabatic regime. As such, it is common to employ a threshold criterion and measure instead the transition time, \hat{t}_{th} , which is the time it takes for an order parameter to reach a given threshold after passing λ_c . The crossover point at the transition time, $\varepsilon(\hat{t}_{\text{th}})$, is similarly defined. For a sufficiently small threshold value, it is assumed that \hat{t}_{th} is a good approximation for \hat{t} . While this method is successful in showing the power-law scaling of \hat{t}_{th} and $\varepsilon(\hat{t}_{\text{th}})$ as a function of τ_q [5, 10, 12, 28, 32, 37, 41], it remains unclear whether the inherent deviation between \hat{t} and \hat{t}_{th} does not lead to any significant effects on the scaling of the KZM quantities for any generic quench protocols.

In this paper, we report an intermediate regime separating the breakdown and validity of the KZM appearing in open systems under a finite quench protocol depicted in Fig. 1(a). In this regime, the transition time follows the power-law scaling predicted by the KZM even though

* rjara@nip.upd.edu.ph

† jcosme@nip.upd.edu.ph

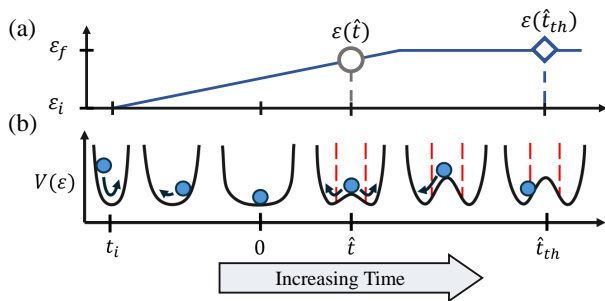


FIG. 1. Sketch of a generic open system undergoing a continuous phase transition. (a) A finite ramp protocol is applied on a system initialized in the normal phase. (b) The quench modifies the effective potential experienced by the system represented by the ball. This pushes the system to enter a symmetry-broken phase at \hat{t} after the ramp passes the critical point $\varepsilon(t=0)=0$. The transition, however, is only detected after the system’s order parameter reaches the set threshold value, marked by vertical dashed lines, at \hat{t}_{th} .

the system appears to relax after the quench has terminated, as illustrated in Fig. 1(b). As we will show later, this regime manifests precisely due to the dissipation exacerbating the deviation between the freeze-out time and the transition time, leading to a delay in the detection of the phase transition, as schematically represented in Fig. 1(b). We demonstrate using the open Dicke model (DM) [42, 43] and its one-dimensional lattice extension, the open Dicke lattice model (DLM) [44] that the range of τ_q where we observe this “delayed” KZM is a generic feature of open systems with finite dissipation strength, κ . We also show that the delayed KZM is more prominent near criticality and that its signatures become more significant for large threshold values for an order parameter. Thus, our paper highlights subtleties of the KZM in open systems in finite quench scenarios relevant to experiments.

The paper is structured as follows. In Sec. II, we introduce a minimal system that can exhibit the delayed KZM when quenched at intermediate values of τ_q . By deriving an effective potential for the minimal system, we show that the phenomenon is due to a relaxation mechanism induced by the dissipation of the system. Then, using the open DM and open DLM as a test bed, we demonstrate in Sec. III that the delayed KZM is a generic feature of open systems under a finite quench and that the phenomenon becomes more prominent near criticality. In Sec. IV, we explore how the deviations brought by the delayed KZM can be further exacerbated with large thresholds for order parameters and propose an alternative method for measuring the transition time beyond the threshold-based criterion. We provide a summary and possible extensions of our work in Sec. V.

II. DELAYED KZM: THEORY

Consider a generic open system with a continuous phase transition that is described by the Lindblad master equation [45],

$$\partial_t \hat{\rho} = -i \left[\hat{H}(\varepsilon(t)) / \hbar, \hat{\rho} \right] + \mathcal{D} \hat{\rho}, \quad (2)$$

where $\mathcal{D} \hat{\rho} = \sum_{\ell} \kappa_{\ell} \left(2 \hat{L}_{\ell} \hat{\rho} \hat{L}_{\ell}^{\dagger} - \left\{ \hat{L}_{\ell}^{\dagger} \hat{L}_{\ell}, \hat{\rho} \right\} \right)$ is the dissipator and $\hat{H}(\varepsilon(t))$ is the time-dependent Hamiltonian of the system. The system undergoes a phase transition from a normal phase (NP), in which the global symmetry of the system is preserved, to a symmetry-broken phase via a finite quench protocol,

$$\varepsilon(t) = \begin{cases} t/\tau_q & t_i \leq t \leq \varepsilon_f \tau_q \\ \varepsilon_f & \varepsilon_f \tau_q < t \leq t_f \end{cases} \quad (3)$$

where $t_i = -\tau_q$ and t_f are the initial and final time of the quench. In the following, we demonstrate that if the system can be approximated as or mapped onto an effective coupled oscillator system (COS), with at least one dissipative channel, as sketched in Fig. 2(a), then we should observe a finite range of τ_q where the deviation between \hat{t} and \hat{t}_{th} becomes significant enough that we get a contradictory behavior between the scaling of the transition time and crossover point. To observe the dynamics of the systems considered in this paper, we will use a mean-field approach and assume that for any operators, \hat{A} and \hat{B} , $\langle \hat{A} \hat{B} \rangle \approx \langle \hat{A} \rangle \langle \hat{B} \rangle$. This allows us to treat any operators as complex numbers and use the notation $A \equiv \langle \hat{A} \rangle$. We numerically integrate the systems’ mean-field equations in Appendix A using a standard fourth-order Runge Kutta algorithm with a time step of $\omega \Delta t = 0.01$, where ω is a frequency associated to the dissipative channel, as we will show later.

The Hamiltonian of the COS is

$$\frac{\hat{H}^{COS}}{\hbar} = \omega \hat{a}^{\dagger} \hat{a} + \omega_0 \hat{b}^{\dagger} \hat{b} + \lambda(t) (\hat{a}^{\dagger} + \hat{a}) (\hat{b} + \hat{b}^{\dagger}), \quad (4)$$

where ω and ω_0 are the transition frequencies associated with the bosonic modes \hat{a} and \hat{b} , respectively, and $\lambda(t)$ is the coupling strength between the two modes. The \hat{a} mode is subject to dissipation, which is captured in the master equation by the dissipator $\mathcal{D} \hat{\rho} = \kappa (2 \hat{a} \hat{\rho} \hat{a}^{\dagger} - \{ \hat{a}^{\dagger} \hat{a}, \hat{\rho} \})$. The COS has an extensive application in multiple settings, such as—but not limited—to cavity-magnon systems [46, 47], atom-cavity systems [42, 43, 48, 49], and spin systems [50, 51].

The open COS has two phases: the NP which corresponds to a steady state with $a = b = 0$, and an unbounded state where both modes exponentially diverge as $t \rightarrow \infty$ [42]. When nonlinearity is present, the unbounded state can be associated with a symmetry-broken phase, in which the modes choose a new steady state

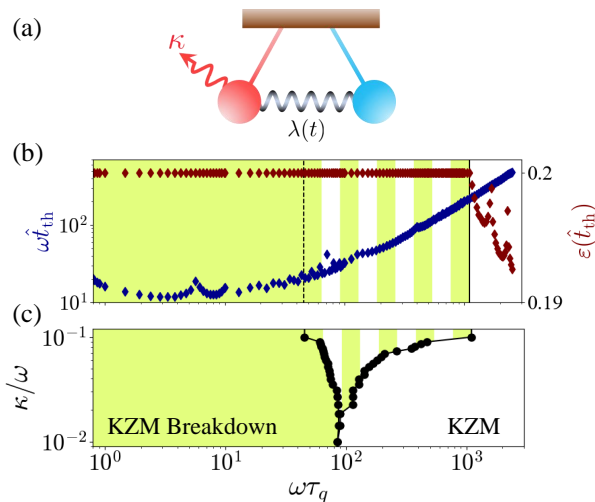


FIG. 2. (a) Sketch of the open COS. (b) Scaling of \hat{t}_{th} and $\varepsilon(\hat{t}_{\text{th}})$ as a function of τ_q for $\kappa = 0.1\omega$. The vertical dashed line corresponds to $\tau_{q,c}$, while the solid line corresponds to $\tau_{q,c}^*$. (c) Boundary of the delayed KZM as a function of κ . The remaining parameters are set to $\varepsilon_f = 0.2$ and $|a|_{\text{th}}^2 = 2$.

depending on their initial values. These two states are separated by the critical point [42]:

$$\lambda_c = \frac{1}{2} \sqrt{\frac{\omega_0}{\omega} (\kappa^2 + \omega^2)}. \quad (5)$$

To show that the COS is a minimal model that can exhibit the KZM and its subsequent breakdown at small τ_q , we consider its dynamics as it transitions from the NP to the unbounded state. We do this by initializing the system near the steady state of NP, $a_0 = -b_0 = 0.01$. We then apply the quench protocol in Eq. (3) onto the COS and track the dynamics of the occupation number of the \hat{a} mode, $|a|^2$. We finally determine \hat{t}_{th} by identifying the time it takes for $|a|^2$ to reach the threshold value, $|a|_{\text{th}}^2$, after the ramp passes $\varepsilon(t=0) = 0$. The crossover point at the transition time is then inferred back from \hat{t}_{th} using Eq. (3). We present in Fig. 2(b) the scaling of \hat{t}_{th} and $\varepsilon(\hat{t}_{\text{th}})$ as a function of τ_q . We can observe that for large τ_q , or slow quench, all relevant quantities follow the power-law scaling predicted by the KZM. As we decrease τ_q , $\varepsilon(\hat{t}_{\text{th}})$ begins to saturate at a larger critical quench time, $\tau_{q,c}^*$, than \hat{t}_{th} , as indicated by the solid line in Fig. 2(b). Finally, as $\tau_q \rightarrow 0$, \hat{t}_{th} approaches a constant value after passing another critical quench time, $\tau_{q,c}$, denoted in Fig. 2(b) as a dashed line. Note that the fluctuations in the scaling of \hat{t}_{th} and $\varepsilon(\hat{t}_{\text{th}})$ can be attributed to the mean-field approach, which neglects any quantum fluctuation in the system's dynamics. The scaling behavior of \hat{t}_{th} and $\varepsilon(\hat{t}_{\text{th}})$ implies that within the range $\tau_{q,c} < \tau_q \leq \tau_{q,c}^*$, there exists an intermediate regime between the true breakdown and the validity of the KZM, wherein the KZM remains valid even though the system appears to relax well after the quench has terminated.

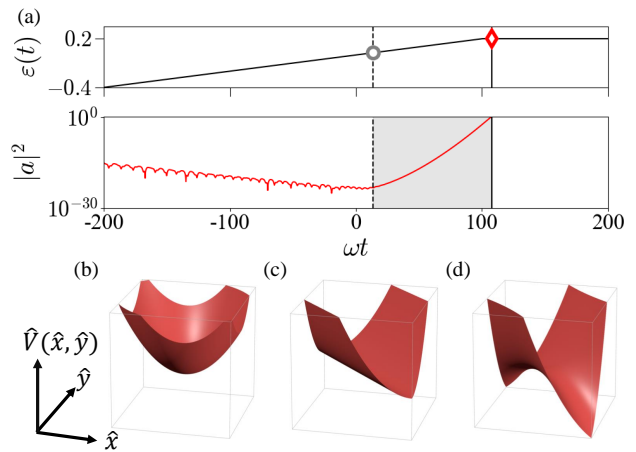


FIG. 3. (a) (top panel) Ramp protocol for $\omega\tau_q = 500$ and $\varepsilon_f = 0.2$. The circle point indicates $\varepsilon(\hat{t})$ while the diamond point marks $\varepsilon(\hat{t}_{\text{th}})$. Bottom panel: Exemplary dynamics of $|a|^2$ in the τ_q -regime of the delayed KZM for $\kappa = 0.1\omega$. The vertical dashed lines correspond to $\omega\hat{t}$, while the solid lines represent $\omega\hat{t}_{\text{th}}$ for a threshold of $|a|_{\text{th}}^2 = 2$. (b), (c) potential surface of the open COS for (b) $\varepsilon(t) < 0$, (c) $\varepsilon(t) = 0$, and (d) $\varepsilon(t) > 0$.

As shown in Fig. 2(c), this intermediate regime vanishes as $\kappa \rightarrow 0$, highlighting that this is a dissipation-induced effect.

We can understand this apparent contradiction between the scaling of the \hat{t}_{th} and $\varepsilon(\hat{t}_{\text{th}})$ by looking at the dynamics of $|a|^2$ as the ramp crosses over $\varepsilon = 0$. In Fig. 3(a), we present an exemplary dynamics of $|a|^2$ in the logarithmic scale for the regime $\tau_{q,c} < \tau_q \leq \tau_{q,c}^*$. Notice that before the system enters the unbounded state, $|a|^2$ first exponentially decays towards its steady state, indicating that the system does not freeze in the impulse regime. This dynamics is reminiscent of systems relaxing towards the global minimum of their energy surface due to dissipation, as sketched in Fig. 1(b). We can further establish this connection by obtaining the potential surface of the COS, which we can do by substituting the pseudoposition and momentum operators for the \hat{a} mode,

$$\hat{x} = \frac{1}{\sqrt{2\omega}} (\hat{a}^\dagger + \hat{a}), \quad \hat{p}_x = i\sqrt{\frac{\omega}{2}} (\hat{a}^\dagger - \hat{a}), \quad (6)$$

and the \hat{b} mode,

$$\hat{y} = \frac{1}{\sqrt{2\omega_0}} (\hat{b}^\dagger + \hat{b}), \quad \hat{p}_y = \sqrt{\frac{\omega_0}{2}} (\hat{b}^\dagger - \hat{b}), \quad (7)$$

back to Eq. (4). Note that for the remainder of this section, we set $\hbar = 1$ for brevity. With this substitution, the COS Hamiltonian becomes

$$\hat{H}^{\text{COS}} = \frac{\hat{p}_x^2}{2} + \frac{\hat{p}_y^2}{2} + \hat{V}(\hat{x}, \hat{y}), \quad (8)$$

where

$$\hat{V}(\hat{x}, \hat{y}) = \frac{1}{2}\omega^2\hat{x}^2 + \frac{1}{2}\omega_0^2\hat{y}^2 + 2\sqrt{\omega\omega_0}\lambda\hat{x}\hat{y} \quad (9)$$

is the effective potential of the COS in the closed system limit, $\kappa = 0$. In this limit, the potential surface has a global minimum at $\hat{x} = \hat{y} = 0$ when $\lambda < \lambda_c = \sqrt{\omega\omega_0}/2$, as shown in Fig. 3(b). It then loses its global minimum when $\lambda = \lambda_c$ as sketched in Fig. 3(c). Finally, the global minimum becomes a saddle point when $\lambda > \lambda_c$, as shown in Fig. 3(d). Note that in the presence of dissipation, the COS effective potential only becomes modified such that the critical point becomes Eq. (5), while the structure of the potential surface remains the same due to Eq. (8) being quadratic.

With the above picture, we can now interpret the relaxation mechanism observed in Fig. 3(a) as follows. Suppose that we initialize our system such that $\lambda < \lambda_c$ and the initial states of \hat{a} and \hat{b} modes are close to the global minimum of \hat{V} . In the mean-field level, if $\kappa = 0$, we can expect that the system will oscillate around the global minimum of \hat{V} as we increase λ using the finite ramp protocol defined in Eq. (3), together with the modification of the COS potential surface. As we cross λ_c , the global minimum of \hat{V} becomes a saddle point. As such, any deviation of the initial state from the origin would eventually push the system to either the positive \hat{x} and $-\hat{y}$ direction or vice versa, signaling the spontaneous symmetry breaking of the system.

In the presence of dissipation, however, the system can still relax to the global minimum before the quench reaches λ_c for sufficiently large quench timescales $\tau_q > \tau_{q,c}$. As a result, the slow deformation of the effective potential allows for the system to remain near $a = b = 0$ even after passing the critical point where the potential loses its global minimum. The nudge from the system's initial state eventually pushes the system towards a new minimum as the quench progresses, signaling the phase transition. This approach, however, only becomes detectable when $|a|^2$ reaches $|a|_{\text{th}}^2$, which occurs only after the linear ramp has terminated. Thus, we observe the saturation of the crossover point at ε_f even though \hat{t}_{th} follows the predicted scaling of the KZM, which hints that the system entered the adiabatic regime within the duration of the ramp. Note that the relaxation mechanism is not present in the closed limit, as hinted by the regime vanishing in Fig. 2(c) as $\kappa \rightarrow 0$. The delay between \hat{t} and \hat{t}_{th} at finite τ_q motivates us to call this phenomenon delayed KZM.

In the next section, we will show that the delayed KZM is a generic feature of open systems that can be mapped onto an effective COS. Moreover, we will demonstrate that not only is the delayed KZM induced purely by dissipation but it also becomes more prominent when the system is quenched near criticality, $\varepsilon_f \approx 0$.

III. DELAYED KZM IN OPEN SYSTEMS

A. Signatures of the delayed KZM

We now test whether the delayed KZM is a generic feature of open systems by considering two fully connected systems: the open DM, schematically represented in Fig. 4(a), and its one-dimensional lattice version, the open DLM, as shown in Fig. 4(b). Both systems are described by the master equation in Eq. (2), with the Hamiltonian of the open DM being [42, 43]

$$\frac{\hat{H}^{\text{DM}}}{\hbar} = \omega \hat{a}^\dagger \hat{a} + \omega_0 \hat{S}^z + \frac{2\lambda(t)}{\sqrt{N}} (\hat{a} + \hat{a}^\dagger) \hat{S}^x, \quad (10)$$

while the Hamiltonian of its M -site lattice version with periodic boundary conditions takes the form [44]

$$\frac{\hat{H}^{\text{DLM}}}{\hbar} = \frac{1}{\hbar} \sum_{\ell}^M \hat{H}_{\ell}^{\text{DM}} - J \sum_{\langle i,j \rangle}^M (\hat{a}_i^\dagger \hat{a}_j + \hat{a}_j^\dagger \hat{a}_i). \quad (11)$$

The open DM has the same dissipator as the open COS, while the dissipator of the open DM is $\mathcal{D}\hat{\rho} = \kappa \sum_{\ell}^M (2\hat{a}_{\ell} \hat{\rho} \hat{a}_{\ell}^\dagger - \{\hat{a}_{\ell}^\dagger \hat{a}_{\ell}, \hat{\rho}\})$ [44]. The open DM describes the dynamics of N two-level systems, represented by the collective spin operators $\hat{S}^{x,y,z}$, coupled to a dissipative bosonic mode, \hat{a} , which in cavity-QED experiments corresponds to a photonic mode [28, 41, 43, 48]. In both systems, ω and ω_0 are the bosonic and spin transition frequencies, respectively, and λ is the spin-boson coupling, while J represents the nearest-neighbor interaction in the open DLM.

In equilibrium, the open DM has two phases: the NP and the superradiant (SR) phase [42, 43]. The NP is characterized by a fully polarised collective spin at the $-z$ direction, i.e. $S^z = -N/2$, and a zero total occupation number, $|a|^2$. Meanwhile, the SR phase is associated with the \mathbb{Z}_2 symmetry breaking of the system, leading to a nonzero S^x and $|a|^2$, with S^x (a) picking a random sign (phase) from the two degenerate steady states of the system [43]. The two phases are separated by the same critical point as the open COS [43]. Under a finite quench, however, the open DM exhibits nontrivial dynamics as it transitions from the NP to the SR phase. We present in Figs. 4(c)-4(e) an exemplary dynamics of the total occupation number, $|a|^2$, and the phase of the bosonic mode, φ , and S^x of the open DM for $\omega\tau_q = 1000$. We initialized the system near the steady state of the NP, where the initial values of the bosonic mode are $a = 0.01$, while the collective spin operators are

$$S^x(t_i) = \frac{N}{2} \delta, \quad S^y(t_i) = 0, \quad S^z(t_i) = -\frac{N}{2} \sqrt{1 - \delta^2}, \quad (12)$$

where δ is a perturbation set to $\delta = 0.01$. We can observe that when the system is in the NP, the occupation number approaches the NP steady state, $a = 0$, which

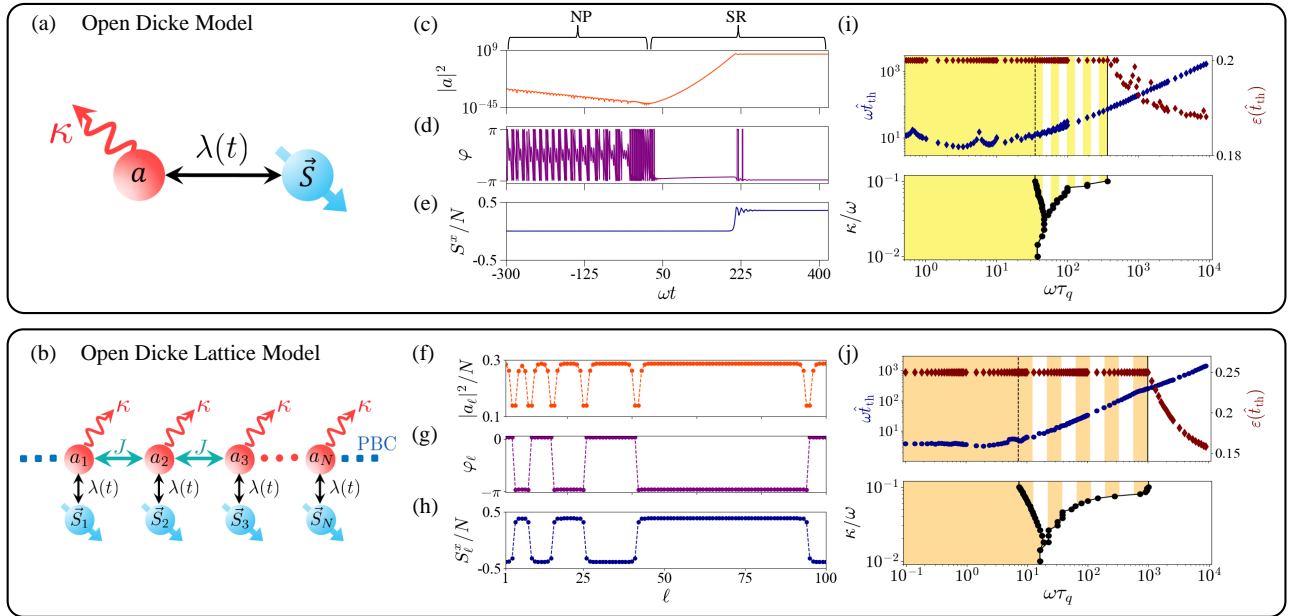


FIG. 4. (a), (b) Sketch of the (a) open Dicke model and the (b) open Dicke lattice model with periodic boundary condition. (c)-(e) Exemplary dynamics of the (c) occupation number, (d) phase of the \hat{a} mode, and (e) S^x of the quenched open Dicke model for $\omega\tau_q = 1000$ and $\varepsilon_f = 0.2$. (f)-(h) Exemplary steady-state spatial distribution of the (f) occupation number, (g) phase of the \hat{a}_ℓ mode, and (h) S_ℓ^x of the open Dicke lattice model in the SR phase. (i)-(j) Signatures of the delayed KZM for the (i) open DM and (j) open DLM. Top panel: Scaling of \hat{t}_{th} as a function of τ_q for $\kappa = 0.1\omega$. The vertical dashed lines represent $\tau_{q,c}$, while the solid lines corresponds to $\tau_{q,c}^*$. Bottom panel: The boundary of the delayed KZM regime as a function of κ . The remaining parameters are set to $\varepsilon_f = 0.2$ and $|a|_{\text{th}}^2 = 2$ for the open DM, and $J = 0.1\omega$, $\varepsilon_f = 0.25$, and $|a|_{\text{th}}^2/M = 2$, with $M = 500$ sites, for the open DLM.

is consistent with our predicted behavior from the potential surface interpretation of phase transition in an open system, which we describe in Sec. II. In addition, the phase of the bosonic mode oscillates from $-\pi$ to π , while the S^x remains close to $S^x = 0$. As $\varepsilon(t) > 0$ at $t > 0$, the system enters the SR phase, which results in φ spontaneously admitting a finite value as the $|a|^2$ starts to exponentially grow until $t = \varepsilon_f\tau_q$, where the ramp terminates. At that point, the $|a|^2$ finally saturates at the steady state of the SR phase. Meanwhile, the transition of S^x from its behavior in the NP to the SR phase only becomes prominent at a later time. We will further expand on the implication of the behavior of these order parameters later in Sec. IV.

As for the open DLM, for small values of J , the interaction between the open DMs modifies the λ_c into a critical line [44]:

$$\lambda_c = \frac{1}{2} \sqrt{\omega_0(\omega - 2J) \left(1 + \frac{\kappa^2}{(\omega - 2J)^2} \right)}. \quad (13)$$

Moreover, suppose that we drive the open DLM from the NP to the SR phase using a finite quench after initializing it near the steady state of NP. Specifically, we initialize the collective spins at $S_\ell^{x,y,z} = S^{x,y,z}(t = t_i)$, while the bosonic modes are initialized at the vacuum state, which can be represented as a complex Gaussian vari-

able $a_\ell = \frac{1}{2} (\eta_\ell^R + \eta_\ell^I)$, where $\eta_\ell^{R,I}$ are random numbers sampled from a Gaussian distribution satisfying $\langle \eta_\ell^i \rangle = 0$ and $\langle \eta_\ell^i \eta_m^j \rangle = \delta_{i,j} \delta_{\ell,m}$ for $i, j = R, I$ [52]. Then, as the system enters the SR phase, each site can independently pick between the two degenerate steady states available, allowing for the formation of domains and point defects, the number of which depends on the correlation length of the system. We present in Figs. 4(f)-4(h) the exemplary spatiotemporal dynamics of $|a_\ell|^2$, φ_ℓ , and S_ℓ^x of the open DLM after doing a finite quench towards the SR phase. We can observe that the point defects can manifest either as dips in the occupation number, phase slips in the spatial profile of φ_ℓ , or domain walls in S_ℓ^x . Note that the defect number N_d follows the predicted KZM power-law scaling with τ_q , which we demonstrate in Appendix B. Since the notion of topological defects is well-defined in the open DLM, it serves as a good test bed for the delayed KZM for systems with short-range interaction. This is in addition to the open DM, which has been experimentally shown to exhibit signatures of the KZM [28] despite the open question of its nonequilibrium universality class [53, 54].

We now present in Figs. 4(i) and 4(j) the scaling of \hat{t}_{th} and $\varepsilon(\hat{t}_{\text{th}})$ as a function of τ_q for the open DM and open DLM, respectively. Similar to the COS, the \hat{t}_{th} for both systems is inferred from the total occupation

number, which for the open DLM is explicitly defined as $|a|^2 = \sum_\ell |a_\ell|^2$. Notice that both systems exhibit the signatures of the delayed KZM, where \hat{t}_{th} continues with its KZM power-law scaling as $\varepsilon(\hat{t}_{\text{th}})$ saturates for intermediate values of τ_q . They also exhibit the closing of the boundary of the delayed KZM as we decrease κ . We can understand the emergence of the delayed KZM in these two systems by noting that the open DM can be mapped exactly into the COS in the thermodynamic limit, $N \rightarrow \infty$. We can do this by applying the approximate Holstein-Primakoff representation (HPR) [42, 43],

$$\hat{S}^z = \frac{N}{2}, \quad \hat{S}^- = \sqrt{N} \left(\sqrt{1 - \frac{\hat{b}^\dagger \hat{b}}{N}} \right) \hat{b} \approx \sqrt{N} \hat{b}, \quad (14)$$

on Eq. (10) to reduce it onto the COS Hamiltonian in Eq. (4) up to a constant term.

Meanwhile, we can transform the open DLM into a set of COS in the thermodynamic limit by first substituting the approximate HPR of the collective spins to Eq. (11), noting that $\hat{S}^{z,\pm} \rightarrow \hat{S}_\ell^{z,\pm}$ and $\hat{b} \rightarrow \hat{b}_\ell$ [44]. This leads to a Hamiltonian of the form,

$$\frac{\hat{H}^{\text{DLM}}}{\hbar} \approx \frac{1}{\hbar} \sum_\ell \hat{H}_\ell^{\text{COS}} - J \sum_{\langle i,j \rangle} \left(\hat{a}_i^\dagger \hat{a}_j + \hat{a}_j^\dagger \hat{a}_i \right). \quad (15)$$

We then perform a discrete Fourier transform,

$$\hat{a}_k = \frac{1}{\sqrt{M}} \sum_\ell e^{ik\ell} \hat{a}_\ell, \quad \hat{b}_k = \frac{1}{\sqrt{M}} \sum_\ell e^{ik\ell} \hat{b}_\ell, \quad (16)$$

on Eq. (15) to obtain an effective Hamiltonian,

$$\frac{\hat{H}^{\text{DLM}}}{\hbar} \approx \frac{1}{\hbar} \sum_k \hat{H}_k^{\text{OM}}, \quad (17)$$

where

$$\frac{\hat{H}_k^{\text{OM}}}{\hbar} = \omega_k \hat{a}_k^\dagger \hat{a}_k + \omega_0 \hat{b}_k^\dagger \hat{b}_k + \lambda \left(\hat{a}_k^\dagger \hat{b}_k + \hat{a}_{-k} \hat{b}_k + \text{H.c.} \right) \quad (18)$$

is the Hamiltonian of each uncoupled oscillator at the momentum mode k and $\omega_k = \omega - 2J \cos(k)$. In this form, we can easily observe that the open DLM has a similar structure to the COS, with the similarity being more apparent at the zero-momentum mode:

$$\frac{\hat{H}_0^{\text{OM}}}{\hbar} = (\omega - 2J) \hat{a}_0^\dagger \hat{a}_0 + \omega_0 \hat{b}_0^\dagger \hat{b}_0 + \lambda \left(\hat{a}_0^\dagger + \hat{a}_0 \right) \left(\hat{b}_0^\dagger + \hat{b}_0 \right). \quad (19)$$

These results show that the signatures of the delayed KZM can appear not only in the open DM but also in the open DLM, where both short-range interactions between the sites and multiple degenerate steady states are present in the system. As such, we confirm that the delayed KZM is a generic feature of open systems under a finite quench that can be mapped onto a COS, regardless of the interaction present in the system.

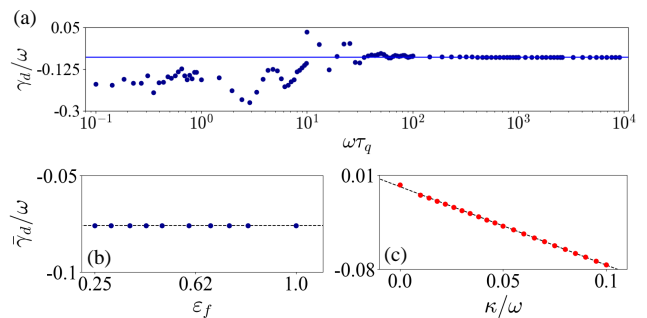


FIG. 5. (a) Dependence of the occupation number decay rate of the open DLM on τ_q for $\varepsilon_f = 0.25$ and $\kappa = J = 0.1\omega$. The solid line corresponds to the average value of γ_d from $\omega\tau_q = 10^2$ to $\omega\tau_q = 10^4$. (b), (c) $\bar{\gamma}_d$ as a function of (b) ε_f for $\kappa = 0.1\omega$ and (c) κ for $\varepsilon_f = 0.25$. The dashed lines correspond to the best-fit lines.

Since we have shown the generality of the delayed KZM on open systems, we now explore in greater detail the dissipative and near-critical nature of the delayed KZM in Sec. III B.

B. Dissipative and critical nature of the delayed KZM

In Sec. II, we have claimed that the dissipation is responsible for the relaxation mechanism that leads to the emergence of the delayed KZM. This is also corroborated by the disappearance of the delayed KZM regime in the closed limit, implying that the phenomenon appears only at finite dissipation strength, κ . We now explicitly demonstrate that this claim is true for any generic open systems by calculating the decay rate of the total occupation number, γ_d , as the system approaches the critical point. We will then identify how γ_d scales with ε_f and κ . For the rest of this section, we will only consider the open DLM, although our results here should apply as well for both the COS and the open DM.

To determine the γ_d of the open DLM for a given κ and ε_f , we calculate the slope of the best-fit line of the logarithm of $|a|^2$ within the time interval $[-0.75\tau_q, 0]$. The chosen time window is arbitrary, but it ensures that the γ_d is inferred within the duration that the system is in the impulse regime. We show in Fig. 5(a) the dependence of γ_d with the quench time. We can observe that γ_d is constant for large values of τ_q . As we decrease τ_q , however, γ_d begins to fluctuate and eventually decreases to a much lower value. We attribute the deviation of γ_d from its constant value on the errors incurred in the best-fit line of $\ln |a|^2$ for small values of τ_q . In particular, since we only considered a simulation time step of $\omega\Delta t = 0.01$, the small time window for these values of τ_q leads to smaller sets of data points for $|a|^2$, resulting to an overall poorer fit. Due to this consideration, we only considered the data points from $\omega\tau_q = 10^2$ to $\omega\tau_q = 10^4$

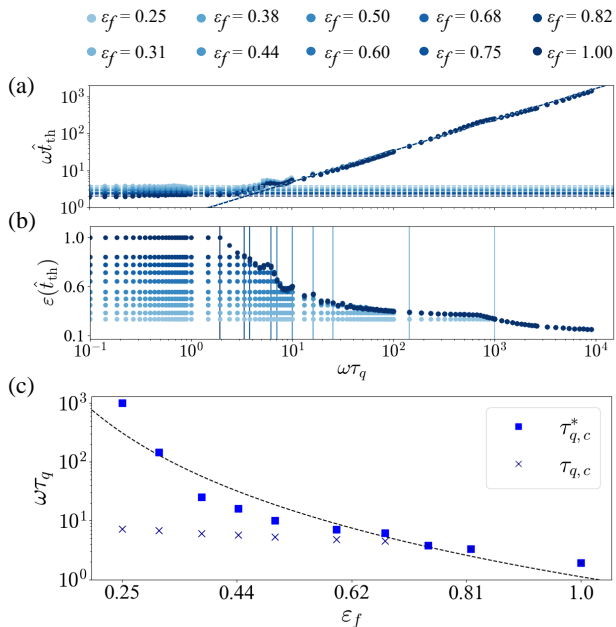


FIG. 6. (a)-(b) Scaling of (a) \hat{t}_{th} and (b) $\varepsilon(\hat{t}_{\text{th}})$ of the open DLM as a function of τ_q for different ε_f . The dashed lines in (a) correspond to the best-fit lines of \hat{t}_{th} for fast and slow quenches, with their intersections marking $\tau_{q,c}$. Meanwhile, the dashed lines in (b) denote $\tau_{q,c}^*$. (c) Borders of the delayed KZM regime as a function of ε_f . The dashed line corresponds to the best-fit line of $\tau_{q,c}^*$. The remaining parameters are $\kappa = J = 0.1\omega$, and $|a|_{\text{th}}^2/M = 2$, with $M = 500$ sites.

in calculating the average value of the decay rate with $\tau_q, \bar{\gamma}_d$.

We now present in Figs. 5(b) and 5(c) the behavior of $\bar{\gamma}_d$ as a function of ε_f and κ , respectively. We can observe that $\bar{\gamma}_d$ remains constant for all values of ε_f , implying that the average decay rate of $|a|^2$ is independent of the quench protocol used in the system. Meanwhile, $\bar{\gamma}_d$ has an inverse relationship with κ , demonstrating that the relaxation mechanism responsible for the delayed KZM is indeed a direct result of dissipation allowing the initial occupation number in the dissipative bosonic mode to leak out of the system as it remains in the impulse regime. For completeness, we check the linear dependence of $\bar{\gamma}_d$ with κ by fitting a line on it and calculating the square of its Pearson correlation coefficient, R^2 . By doing this, we obtain $R^2 = 0.9996$, which indicates a great fit between the best-fit line and the data points.

Given that ε_f do not alter the behavior of the decay rate of $|a|^2$, it is natural to ask whether varying ε_f has any significant effect as well on the scaling of \hat{t}_{th} and $\varepsilon(\hat{t}_{\text{th}})$, and on the signatures of the delayed KZM. We answer the first question in Figs. 6(a) and 6(b), where we show the scaling of \hat{t}_{th} and $\varepsilon(\hat{t}_{\text{th}})$, respectively, with τ_q for different values of ε_f . We can see that varying ε_f does not significantly change the scaling of the KZM quantities considered. However, the $\tau_{q,c}^*$, shown as solid lines in

Fig. 6(b), increases significantly as we decrease ε_f . This modification on $\tau_{q,c}^*$ becomes more apparent in Fig. 6(c), where we show the scaling of $\tau_{q,c}$ and $\tau_{q,c}^*$ as a function of ε_f . Notice that both quantities are inversely proportional to ε_f , with $\tau_{q,c}^*$ dropping faster than $\tau_{q,c}$ as $\varepsilon \rightarrow \infty$. As a result, the delayed KZM regime vanishes for large ε_f , highlighting that its signatures become more apparent for strongly dissipative systems quenched near criticality. We finally note that $\tau_{q,c}^*$ follows a power-law scaling as evidenced by the power-law fit curve shown in Fig. 6(c). In particular, since $\tau_{q,c}^*$ becomes the true critical quench time separating the breakdown and validity of the KZM at large ε_f , we expect that it should follow the power-law scaling [40]

$$\tau_{q,c}^* \propto \varepsilon_f^{-(vz+1)}, \quad (20)$$

which we show to be the case in Appendix B.

So far, we have shown that the presence of the delayed KZM leads to a significant deviation between the true freeze-out time, \hat{t} , and the transition time, \hat{t}_{th} . Given that the delayed KZM becomes more prominent near criticality at strong dissipation, we now address in the next section how the threshold-based criterion for determining \hat{t}_{th} contributes to the deviation and whether a more accurate method can be used to measure \hat{t} .

IV. TRANSITION TIME MEASUREMENT

The threshold value used to determine the transition time plays a role in the delay between \hat{t} and \hat{t}_{th} . In particular, we can expect a longer delay for larger $|a|_{\text{th}}^2$ since the system's order parameter has to reach a larger threshold value before being detected. This intuition prompts the question of whether decreasing the threshold value has any effect on the scaling of \hat{t}_{th} and $\varepsilon(\hat{t}_{\text{th}})$, and as to whether it can suppress the deviation brought by the delayed KZM, and thus its signatures.

We answer the first question in Figs. 7(a) and 7(b), where we present the scaling of \hat{t}_{th} and $\varepsilon(\hat{t}_{\text{th}})$, respectively. For this part, while we only consider the open DM, the results here should apply to the COS and the open DLM as well. We can observe that the scaling of \hat{t}_{th} and $\varepsilon(\hat{t}_{\text{th}})$ do not significantly change as we increase the threshold value. In particular, while the \hat{t}_{th} is only shifted by a constant value as $|a|_{\text{th}}^2$ increases, both KZM quantities considered eventually collapse in a single scaling as $\tau_q \rightarrow \infty$. As for the boundaries of the delayed KZM regime, we can observe in Fig. 7(c) that the gap between $\tau_{q,c}$ and $\tau_{q,c}^*$ widens as we increase $|a|_{\text{th}}^2$, implying that the delayed KZM becomes more prominent at large $|a|_{\text{th}}^2$.

We can understand the widening of the delayed KZM regime for large $|a|_{\text{th}}^2$ by noting that in an ideal setup where \hat{t} can be accurately identified, the gap between $\tau_{q,c}$ and $\tau_{q,c}^*$ vanishes, and thus following the prediction in Ref. [40], $\tau_{q,c} = \tau_{q,c}^* = \hat{t}/\varepsilon_f$. Since for any threshold-

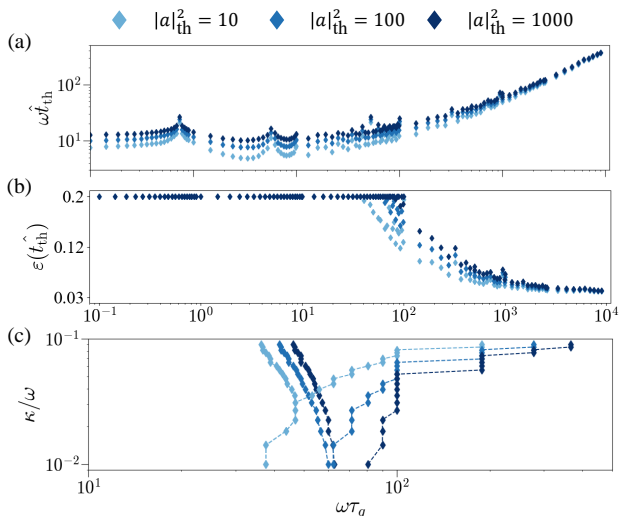


FIG. 7. (a), (b) Scaling of (a) \hat{t}_{th} and (b) $\varepsilon(\hat{t}_{\text{th}})$ of the open DM as a function of τ_q for different values of $|a|_{\text{th}}^2$. (c) Boundary of the delayed KZM regime as a function of κ for different $|a|^2$. The remaining parameters are set to $\varepsilon_f = 0.2$ and $\kappa = 0.1\omega$.

based criterion, $\tau_{q,c}^* = \hat{t}_{\text{th}}/\varepsilon_f$ and $\tau_{q,c} \neq \tau_{q,c}^*$ for large κ and small ε_f , then

$$\tau_{q,c}^* - \tau_{q,c} = \frac{1}{\varepsilon_f} (\hat{t}_{\text{th}} - \hat{t}) \quad (21)$$

Let us assume that within the time interval $[\hat{t}, \varepsilon_f \tau_q]$, the total occupation is exponentially growing such that $|a|^2 \propto \exp(\gamma_g t)$, where γ_g is the growth rate of the total occupation number. This assumption is supported by Fig. 4(c), where the $|a|^2$ of the open DM exponentially grows from the minimum value to its saturation value. With this assumption, we can infer that $\hat{t}_{\text{th}} \propto \ln |a|_{\text{th}}^2 / \gamma_g$ and $\hat{t} \propto \ln |a|_{\text{min}}^2 / \gamma_g$, where $|a|_{\text{min}}^2$ is the minimum value of the total occupation number. Thus,

$$\tau_{q,c}^* - \tau_{q,c} \propto \frac{1}{\varepsilon_f \gamma_g} (\ln |a|_{\text{th}}^2 - \ln |a|_{\text{min}}^2). \quad (22)$$

which implies that we can suppress the signatures of the delayed KZM by setting $|a|_{\text{th}}^2$ close to $|a|_{\text{min}}^2$.

Now, determining an optimal threshold value that suppresses the signatures of the delayed KZM may be difficult to achieve as it requires prior knowledge of $|a|_{\text{min}}^2$ for arbitrary τ_q . This problem motivates the question of whether an alternative method can be used to infer \hat{t} without relying on any threshold-based criterion. As we have hinted in the dynamics of the phase of the \hat{a} mode of the open DM shown in Fig. 4(d), we can do this by choosing an appropriate order parameter that rapidly reaches its steady state upon the system entering a phase transition. In the case of the open DM, this order parameter corresponds to the boson mode's phase, φ . We demonstrate this method further in Figs. 8(b) and 8(c), where

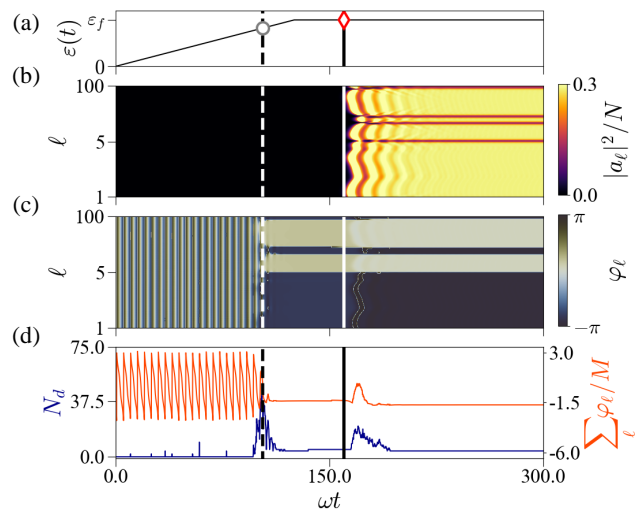


FIG. 8. (a) Ramp protocol for the quench time within the τ_q -regime of the delayed KZM for the open DLM. The circle point marks $\varepsilon(\hat{t})$, while the diamond point denotes $\varepsilon(\hat{t}_{\text{th}})$. (b), (c) Spatiotemporal dynamics of (b) the occupation number $|a_\ell|^2$ and (c) the phase of the \hat{a}_ℓ -mode, φ_ℓ . (d) Exemplary dynamics of the defect number and the site-averaged φ_ℓ . The vertical dashed lines correspond to $\omega \hat{t}$, while the solid lines represent $\omega \hat{t}_{\text{th}}$. The remaining parameters are set to $\varepsilon_f = 1.25$, $\kappa = J = 0.1\omega$, and $|a|_{\text{th}}^2 = 0.05|a|_s^2$, where $|a|_s^2$ is the steady state of $|a|^2$.

we show that for nonzero dimensional systems, like the open DLM, we can use the phase information of the \hat{a}_ℓ modes to extract \hat{t} . As presented in Fig. 8(d), we can do this by determining the time at which either the defect number, N_d , or the site-averaged phase begins to saturate. In the COS level, the inferred \hat{t} for this method would be equivalent to the moment the system picks a new global minimum it would fall onto, signaling phase transition. Thus, we expect that if the system's phase information is available in an experimental setup, such as in Ref. [55], then that can serve as a more sensitive tool for detecting phase transitions compared to threshold-based order parameters that depend on the mode occupations.

V. SUMMARY AND DISCUSSION

In this paper, we extend the Kibble-Zurek mechanism to open systems under a finite quench and report an intermediate regime separating the breakdown and validity of the KZM at fast and slow quench timescales, respectively. This regime manifests as a continuation of the transition time's KZM power-law scaling at τ_q , where the system appears to relax after the quench has terminated. As we have shown using a coupled oscillator system, this phenomenon results from the system's relaxation towards the global minimum of its potential due to dissipation. This mechanism effectively hides the system's crossover to the adiabatic regime, only to be revealed once the system

reaches the arbitrary threshold of the order parameter.

Using the open DM and the open DLM, we have also demonstrated that the delayed KZM is a generic feature of open systems under finite quenches that can be mapped onto a coupled oscillator system. Furthermore, we have shown that the signatures of the delayed KZM, specifically the size of the quench interval where the delayed KZM regime is observed, become more prominent for small values of ε_f , highlighting the dissipative and near-critical nature of this phenomenon. We have discussed the implications of the delayed KZM in the context of the threshold-based criterion typically used in experiments to measure the transition time and proposed an alternative method to measure \hat{t} . Our proposed method only relies on the spatiotemporal information of an appropriate order parameter, such as the defect number and phase information of the system's bosonic modes, thus providing a more sensitive tool for detecting phase transitions.

Our results extend the notion of the KZM to dissipative systems with finite quench protocols beyond the limits of slow and rapid quenches. It also provides a framework on how the manifestation of the KZM can be altered in experimental protocols, wherein limitations in measuring the true AI crossover become more relevant. Since our results are all in the mean-field level, a natural extension of our paper is to verify whether the delayed KZM would survive in the presence of quantum fluctuations. It would also be interesting to test the signatures of the delayed KZM in the quantum regime of the open DM and the open DLM, and further explore their universality classes beyond the mean-field level. These extensions can be readily done in multiple platforms, including, but not limited to, cavity-QED setups [28, 41, 56–58], nitrogen-vacancy center ensembles [44, 59–61], cavity-magnon systems [46, 47], and photonic crystals [62].

ACKNOWLEDGEMENTS

This work was funded by the UP System Balik PhD Program (OVPAA-BPhD-2021-04) and the DOST-SEI Accelerated Science and Technology Human Resource Development Program.

Appendix A: Mean-field Equations of the Considered Systems

To obtain the mean-field equations of the systems considered in the main text, we consider the master equation for the expectation value of an arbitrary operator, \hat{O} ,

$$\partial_t \langle \hat{O} \rangle = i \left\langle \left[\frac{\hat{H}}{\hbar}, \hat{O} \right] + \mathcal{D}\hat{O} \right\rangle, \quad (\text{A1})$$

where \hat{H} is the system's Hamiltonian, and $\mathcal{D}\hat{O} = \sum_{\ell} \kappa_{\ell} \left(2\hat{L}_{\ell}^{\dagger} \hat{O} \hat{L}_{\ell} - \left\{ \hat{L}_{\ell}^{\dagger} \hat{L}_{\ell}, \hat{O} \right\} \right)$ is the dissipator, with \hat{L}_{ℓ}

being the jump operators. We will also let $A = \langle \hat{A} \rangle$ for notation convenience. Using this master equation, the mean-field equation of the open COS is

$$\partial_t a = -i [\omega a + \lambda (b + b^*)] - \kappa a, \quad (\text{A2a})$$

$$\partial_t b = -i [\omega_0 b + \lambda (a + a^*)]. \quad (\text{A2b})$$

As for the open Dicke model, its mean-field equations are

$$\partial_t a = -i \left(\omega a + \frac{2\lambda}{\sqrt{N}} S^x \right) - \kappa a, \quad (\text{A3a})$$

$$\partial_t S^x = -\omega_0 S^y, \quad (\text{A3b})$$

$$\partial_t S^y = \omega_0 S^x - \frac{2\lambda}{\sqrt{N}} (a^* + a) S^z, \quad (\text{A3c})$$

$$\partial_t S^z = \frac{2\lambda}{\sqrt{N}} (a^* + a) S^y. \quad (\text{A3d})$$

Note that for both the open COS and open DLM, the jump operator is given to be $\hat{L}_{\ell} = \hat{L} = \hat{a}$. Finally, the mean-field equations of the open DLM for a jump operator $\hat{L}_{\ell} = \hat{a}_{\ell}$ is

$$\partial_t a_{\ell} = -i \left[\omega a_{\ell} + \frac{2\lambda}{\sqrt{N}} S_{\ell}^x - J (a_{\ell-1} + a_{\ell+1}) \right] - \kappa a_{\ell}, \quad (\text{A4a})$$

$$\partial_t S_{\ell}^x = -\omega_0 S_{\ell}^y, \quad (\text{A4b})$$

$$\partial_t S_{\ell}^y = \omega_0 S_{\ell}^x - \frac{2\lambda}{\sqrt{N}} (a_{\ell} + a_{\ell}^*) S_{\ell}^z, \quad (\text{A4c})$$

$$\partial_t S_{\ell}^z = \frac{2\lambda}{\sqrt{N}} (a_{\ell} + a_{\ell}^*) S^y. \quad (\text{A4d})$$

Appendix B: KZM exponents of the open Dicke Lattice model

One of the key predictions of the KZM is the power-law scaling of the defect number as a function of τ_q [4],

$$N_d \propto \tau_q^{-(D-d) \frac{v}{1+vz}}, \quad (\text{B1})$$

where D and d are the dimensions of the system and the topological defects, respectively. To demonstrate that the open DLM satisfies the predicted KZM scaling for N_d , we present in Fig. 9 the number of phase slips present in the system for a given τ_q and ε_f . We can observe that for large τ_q , N_d follows a power-law scaling behavior with τ_q , emphasizing that the system indeed follows the KZM

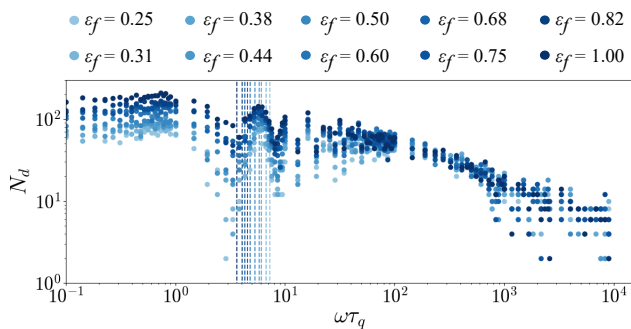


FIG. 9. Scaling of the defect number, N_d , of the open DLM as a function of τ_q , for different values of ε_f . The vertical dashed lines correspond to $\tau_{q,c}$ for a given ε_f . The system parameters are set to $\kappa = J = 0.1\omega$.

at slow quenches, which is consistent with the behavior of \hat{t} and $\varepsilon(\hat{t})$ shown in Figs. 6(a) and 6(b). Notice, however, that as we approach $\tau_{q,c}$, marked by the vertical dashed lines, N_d starts to fluctuate, with the fluctuation becoming more significant as $\varepsilon_f \rightarrow 0$. This behavior is akin to the presaturation regime observed for closed systems under finite quench protocols [35]. As to whether this regime persists in the presence of quantum fluctuation remains an open question. We finally observe the saturation of N_d as $\tau_q \rightarrow 0$, signifying the breakdown of the KZM for small values of τ_q .

Since we have shown that the KZM quantities \hat{t}_{th} , $\varepsilon(\hat{t}_{\text{th}})$, and N_d follow the predicted KZM scaling, for completeness, we now estimate the critical exponents of the open DLM from the power-law exponents of the of these quantities. We do this by assuming that \hat{t}_{th} and N_d follows a generic power-law scaling,

$$\hat{t}_{\text{th}} \propto \tau_q^\alpha, \quad N_d \propto \tau_q^\beta, \quad (\text{B2})$$

within the quench time interval $\omega\tau_q = \omega\tau_{q,c}$ and $\omega\tau_q = 10^4$. From these equations, we can infer from Eqs. (1) and Eq. (B1) that α and β are related to critical exponents v and z by the relations

$$v = \frac{\alpha}{|\beta|}, \quad z = \frac{|\beta|}{1-\alpha}, \quad vz = \frac{\alpha}{1-\alpha}. \quad (\text{B3})$$

We present in Figs. 10(a) and 10(b) the estimated vz as a function of ε_f and κ , respectively, for both the threshold-based transition time and the \hat{t} obtained from the dynamics of the N_d , as described in Sec. IV of the main text. We can see that the threshold-based vz remains relatively constant for all values of ε_f , while the defect-based vz appears to converge to the critical exponent of the Ising universality [63, 64], the universality class of the single Dicke model [65]. We further check whether the two values of vz are consistent with one another by calculating vz as well from the scaling of $\tau_{q,c}^*$ with ε_f , which is given by Eq. (20). We show this in Fig. 10(a) as a solid line, with the grey regions corresponding to the uncertainty due to fitting errors. Notice

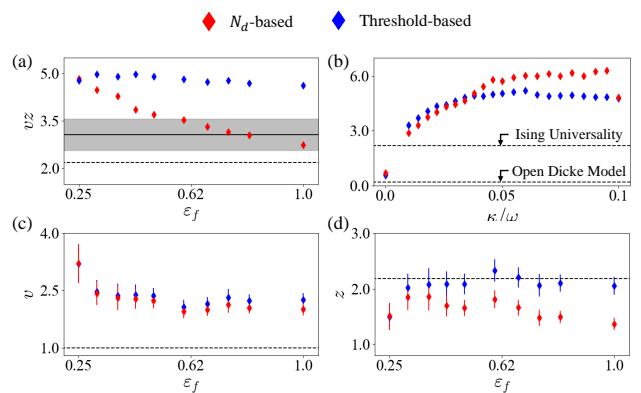


FIG. 10. (a), (b) Calculated vz from the N_d and threshold-based transition time as a function of (a) ε_f for $\kappa = 0.1\omega$ and (b) κ for $\varepsilon_f = 1.25$. The remaining parameter is $J = 0.1\omega$. (c), (d) Estimated critical exponents (c) v and (d) z as a function of ε_f . The dashed lines correspond to the critical exponents of the Ising universality class [63, 64]. The remaining parameters are set to $\kappa = J = 0.1\omega$.

that the value of vz from the defect-based method is consistent with the one obtained from $\tau_{q,c}^*$ for large values of ε_f , while it becomes more consistent with the threshold-based vz for small ε_f . With this picture, the threshold-based vz and $\tau_{q,c}^*$ can be interpreted as the upper and lower bounds for the uncertainty of the open DLM's critical exponents in the mean-field level, respectively.

As for the behavior of the threshold-based and defect-based vz as a function of κ , we can see in Fig. 10(b) that both values of vz decrease as $\kappa \rightarrow 0$. In particular, the vz for both cases approaches the experimental value of vz for the open Dicke model for $\kappa = 1.0\omega$ [28]. This result implies that the system's dissipation modifies the critical exponents of the system, which is consistent with the predictions in Refs. [22] and [23]. Without any specific analytical prediction on how κ modifies the effective critical exponent of the system, we cannot assign a universality class for the open DLM that may apply to any arbitrary dissipation strength.

Given this limitation, we restrict the calculation of the critical exponents for $\kappa = 0.1\omega$. We show in Figs. 10(c) and 10(d) the values of v and z , respectively, for both the defect-based and threshold-based methods. We can observe that the value of v for both cases has a large deviation from the static critical exponent of the Ising universality, which is $v = 1$ [63]. Meanwhile, the value of z for the threshold-based criterion converges to $z \sim 2.183$, which is the dynamic critical exponent of the Ising universality class [64]. As we previously mentioned, we can attribute the deviations of v and z to the dissipation-induced modification of the critical exponents. The accumulated errors on the scaling exponents of N_d , \hat{t}_{th} , and \hat{t}_{N_d} due to the fitting errors may also amplify the deviations of the critical exponents from their expected values. Determining which case has a more significant effect on the values of v and z requires understanding the dynam-

-
- [1] T. W. B. Kibble, *J. Phys. A: Math. Gen.* **9**, 1387 (1976).
- [2] T. W. B. Kibble, *Physics Reports* **67**, 183 (1980).
- [3] W. H. Zurek, *Nature* **317**, 505 (1985).
- [4] A. del Campo and W. H. Zurek, *Int. J. Mod. Phys. A* **29**, 1430018 (2014).
- [5] Q. Ye, S. Wu, X. Jiang, and C. Lee, *J. Stat. Mech.* **2018**, 053110 (2018).
- [6] I. Kang Liu, J. Dziarmaga, S.-C. Gou, F. Dalfovo, and N. P. Proukakis, *Phys. Rev. Research* **2**, 033183 (2020).
- [7] N. Navon, A. L. Gaunt, R. P. Smith, and Z. Hadzibabic, *Science* **347**, 167 (2015).
- [8] L. W. Clark, L. Feng, and C. Chin, *Science* **354**, 606 (2016).
- [9] D. Nagy, G. Szirmai, and P. Domokos, *Eur. Phys. J. D* **48**, 127 (2008).
- [10] K. Shimizu, Y. Kuno, T. Hirano, and I. Ichinose, *Phys. Rev. A* **97**, 033626 (2018).
- [11] J. Dziarmaga and J. M. Mazur, *Phys. Rev. B* **107**, 144510 (2023).
- [12] M. Anquez, B. Robbins, H. Bharath, M. Boguslawski, T. Hoang, and M. Chapman, *Phys. Rev. Lett.* **116**, 155301 (2016).
- [13] V. I. Yukalov, A. N. Novikov, and V. S. Bagnato, *Physics Letters A* **379**, 1366 (2015).
- [14] M. Schmitt, M. M. Rams, J. Dziarmaga, M. Heyl, and W. H. Zurek, *Sci. Adv.* **8**, eabl6850 (2022).
- [15] B.-W. Li, Y.-K. Wu, Q.-X. Mei, R. Yao, W.-Q. Lian, M.-L. Cai, Y. Wang, B.-X. Qi, L. Yao, L. He, Z.-C. Zhou, and L.-M. Duan, *PRX Quantum* **4**, 010302 (2023).
- [16] K. Du, X. Fang, C. Won, C. De, F.-T. Huang, W. Xu, H. You, F. J. Gómez-Ruiz, A. del Campo, and S.-W. Cheong, *Nat. Phys.* [10.1038/s41567-023-02112-5](https://doi.org/10.1038/s41567-023-02112-5) (2023).
- [17] J. J. Mayo, Z. Fan, G.-W. Chern, and A. del Campo, *Phys. Rev. Research* **3**, 033150 (2021).
- [18] A. Keesling, A. Omran, H. Levine, H. Bernien, H. Pichler, S. Choi, R. Samajdar, S. Schwartz, P. Silvi, S. Sachdev, P. Zoller, M. Endres, M. Greiner, V. Vuletić, and M. D. Lukin, *Nature* **568**, 207 (2019).
- [19] N. Chepiga and F. Mila, *Nat Commun* **12**, 414 (2021).
- [20] J.-M. Cui, Y.-F. Huang, Z. Wang, D.-Y. Cao, J. Wang, W.-M. Lv, L. Luo, A. del Campo, Y.-J. Han, C.-F. Li, and G.-C. Guo, *Sci Rep* **6**, 33381 (2016).
- [21] S. Ulm, J. Roßnagel, G. Jacob, C. Degünther, S. T. Dawkins, U. G. Poschinger, R. Nigmatullin, A. Retzker, M. B. Plenio, F. Schmidt-Kaler, and K. Singer, *Nat Commun* **4**, 2290 (2013).
- [22] D. Rossini and E. Vicari, *Phys. Rev. Research* **2**, 023211 (2020).
- [23] P. Hedvall and J. Larson, *Dynamics of non-equilibrium steady state quantum phase transitions* (2017), arXiv:1712.01560.
- [24] A. Zamora, G. Dagvadorj, P. Comaron, I. Carusotto, N. P. Proukakis, and M. H. Szymanska, *Phys. Rev. Lett.* **125**, 095301 (2020).
- [25] R. Puebla, A. Smirne, S. F. Huelga, and M. B. Plenio, *Phys. Rev. Lett.* **124**, 230602 (2020).
- [26] S. M. Griffin, M. Lilienblum, K. T. Delaney, Y. Kumagai, M. Fiebig, and N. A. Spaldin, *Phys. Rev. X* **2**, 041022 (2012).
- [27] A. Bácsi and B. Dóra, *Sci. Rep.* **13**, 4034 (2023).
- [28] J. Klinder, H. Keßler, M. Wolke, L. Mathey, and A. Hemmerich, *Proc Natl Acad Sci USA* **112**, 3290 (2015).
- [29] C. J. O. Reichhardt, A. del Campo, and C. Reichhardt, *Commun Phys* **5**, 1 (2022).
- [30] S. Maegochi, K. Ienaga, and S. Okuma, *Phys. Rev. Lett.* **129**, 227001 (2022).
- [31] W.-C. Yang, M. Tsubota, A. del Campo, and H.-B. Zeng, *Phys. Rev. B* **108**, 174518 (2023).
- [32] H. Wang, X. He, S. Li, H. Li, and B. Liu, *Non-equilibrium dynamics of ultracold lattice bosons inside a cavity* (2022), arXiv:2209.12408.
- [33] F. J. Gómez-Ruiz, D. Subires, and A. del Campo, *Phys. Rev. B* **106**, 134302 (2022).
- [34] F. J. Gómez-Ruiz, J. J. Mayo, and A. del Campo, *Phys. Rev. Lett.* **124**, 240602 (2020).
- [35] H.-C. Kou and P. Li, *Phys. Rev. B* **108**, 214307 (2023).
- [36] J. Goo, Y. Lim, and Y. Shin, *Phys. Rev. Lett.* **127**, 115701 (2021).
- [37] P. M. Chesler, A. M. García-García, and H. Liu, *Phys. Rev. X* **5**, 021015 (2015).
- [38] A. del Campo, G. De Chiara, G. Morigi, M. B. Plenio, and A. Retzker, *Phys. Rev. Lett.* **105**, 075701 (2010).
- [39] F. Gómez-Ruiz and A. del Campo, *Phys. Rev. Lett.* **122**, 080604 (2019).
- [40] H.-B. Zeng, C.-Y. Xia, and A. del Campo, *Phys. Rev. Lett.* **130**, 060402 (2023).
- [41] K. Baumann, C. Guerlin, F. Brennecke, and T. Esslinger, *Nature* **464**, 1301 (2010).
- [42] C. Emary and T. Brandes, *Phys. Rev. E* **67**, 10.1103/PhysRevE.67.066203 (2003).
- [43] F. Dimer, B. Estienne, A. S. Parkins, and H. J. Carmichael, *Phys. Rev. A* **75**, 013804 (2007).
- [44] L. Zou, D. Marcos, S. Diehl, S. Putz, J. Schmiedmayer, J. Majer, and P. Rabl, *Phys. Rev. Lett.* **113**, 023603 (2014).
- [45] H.-P. Breuer and F. Petruccione, *The Theory of Open Quantum Systems* (Oxford University Press, Oxford, England, 2002).
- [46] B. Z. Rameshti, S. V. Kusminskiy, J. A. Haigh, K. Usami, D. Lachance-Quirion, Y. Nakamura, C.-M. Hu, H. X. Tang, G. E. W. Bauer, and Y. M. Blanter, *Physics Reports* **979**, 1 (2022).
- [47] D. Kim, S. Dasgupta, X. Ma, J.-M. Park, H.-T. Wei, L. Luo, J. Doumani, X. Li, W. Yang, D. Cheng, R. H. J. Kim, H. O. Everitt, S. Kimura, H. Nojiri, J. Wang, S. Cao, M. Bamba, K. R. A. Hazzard, and J. Kono, *Observation of the magnonic Dicke superradiant phase transition* (2024), arXiv:2401.01873.
- [48] J. Skulte, P. Kongkhambut, H. Keßler, A. Hemmerich, L. Mathey, and J. G. Cosme, *Phys. Rev. A* **109**, 063317 (2024).
- [49] R. D. Jara Jr., D. F. Salinel, and J. G. Cosme, *Phys. Rev. A* **109**, 042212 (2024).
- [50] M. Calvanese Strinati, L. Bello, A. Pe'er, and E. G. Dalla Torre, *Phys. Rev. A* **100**, 023835 (2019).
- [51] L. Bello, M. Calvanese Strinati, E. G. Dalla Torre, and

- A. Pe'er, *Phys. Rev. Lett.* **123**, 083901 (2019).
- [52] M. K. Olsen and A. S. Bradley, *Opt. Commun.* **282**, 3924 (2009).
- [53] O. L. Acevedo, L. Quiroga, F. J. Rodríguez, and N. F. Johnson, *Phys. Rev. Lett.* **112**, 030403 (2014).
- [54] T. Caneva, R. Fazio, and G. E. Santoro, *Phys. Rev. B* **78**, 104426 (2008).
- [55] H. Keßler, P. Kongkhambut, C. Georges, L. Mathey, J. G. Cosme, and A. Hemmerich, *Phys. Rev. Lett.* **127**, 043602 (2021).
- [56] M. Scigliuzzo, G. Calajò, F. Ciccarello, D. Perez Lozano, A. Bengtsson, P. Scarlino, A. Wallraff, D. Chang, P. Delsing, and S. Gasparinetti, *Phys. Rev. X* **12**, 031036 (2022).
- [57] D. H. White, S. Kato, N. Nemet, S. Parkins, and T. Aoki, *Phys. Rev. Lett.* **122**, 253603 (2019).
- [58] G.-L. Zhu, H. Ramezani, C. Emary, J.-H. Gao, Y. Wu, and X.-Y. Lü, *Phys. Rev. Research* **2**, 033463 (2020).
- [59] R. Amsüss, C. Koller, T. Nöbauer, S. Putz, S. Rotter, K. Sandner, S. Schneider, M. Schramböck, G. Steinhäuser, H. Ritsch, J. Schmiedmayer, and J. Majer, *Phys. Rev. Lett.* **107**, 060502 (2011).
- [60] Y. Liu, J. You, and Q. Hou, *Sci. Rep.* **6**, 21775 (2016).
- [61] T. Astner, S. Nevlacsil, N. Peterschofsky, A. Angerer, S. Rotter, S. Putz, J. Schmiedmayer, and J. Majer, *Phys. Rev. Lett.* **118**, 140502 (2017).
- [62] M. Paternostro, G. S. Agarwal, and M. S. Kim, *New J. Phys.* **11**, 013059 (2009).
- [63] G. Delfino, *J. Phys. A: Math. Gen.* **37**, R45 (2004).
- [64] B. Dammann and J. D. Reger, *EPL* **21**, 157 (1993).
- [65] P. Kirton, M. M. Roses, J. Keeling, and E. G. D. Torre, *Adv. Quantum Technol.* **2**, 1800043 (2019).